#### **CONFERENCE PRE-PRINT**

# ATTAINING TOKAMAK LEVEL PERFORMANCE THROUGH PLASMA DENSITY PROFILE SHAPING AT WENDELSTEIN 7-X

September 30, 2025

S. Bannmann\*a, O. Forda, S.A. Bozhenkova, T. Stangea, R. Lopez-Cansinob, A. Langenberga, M. Wappla, J. Brunnera, G. Fucherta, T. Gonda, D. Hartmanna, J. Knauera, H. Laqua, P. McNeelya, N. Pablanta, E. Pascha, P. Poloskeia, K. Rahbarnia, N. Rusta, R.C. Wolfa and the W7X-Team

- \*: Corresponding author email: sebastian.bannmann@ipp.mpg.de
- a: Max-Planck-Institute for Plasma Physics, Greifswald, Germany
- b: Department of Atomic, Molecular and Nuclear Physics, University of Seville, Spain

# **Abstract**

Progress towards achieving net gain from nuclear fusion is typically characterised by the triple product  $nT\tau$ . Although Stellarators have several benefits for a reactor, such as the inherent steady-state capability and the lack of disruptions, the maximum achieved triple product has historically lagged behind that of equivalent sized Tokamaks. In Wendelstein 7-X, a triple product of  $(1.12\pm0.07)\cdot10^{20}\text{m}^{-3}\text{keVs}$  has recently been achieved and held stable for 1.9s which exceeds several energy confinement times. This marks an important step in Stellarator core plasma performance and puts it in line with H-mode performance in similar sized Tokamaks. The accomplishment was enabled by refining the plasma heating and fueling scenario to shape the density profile. A high core ion temperature is achieved by taking advantage of ITG turbulence suppression in the presence of steep density gradients. The density gradient is created after a spontaneous reduction of anomalous core particle diffusion in plasmas heated and fueled by neutral beam injection. Additional electron-cyclotron-resonance heating raises the achieved triple product but also increases the plasma particle transport, known as density pump-out, which can lead to a collapse of the beneficial density gradient. The emerging balancing task in terms of heating and fueling actuators was explored in magnetic configurations with different values of rotational transform ( $\iota$ ) and mirror ratio. In the best of these, suppression of a series of magnetic islands and optimisation of the heating deposition location resulted in a record Stellarator triple product. The optimised scenario is limited in time only by the technical limits of the neutral beam injectors and control of divertor heat loads. This paper presents the result in the context of the leading magnetic confinement devices along with details of the scenario in which it was achieved.

# 1 Introduction + Methods

Achieving high and stable plasma performance, characterized by a high triple product ( $nT\tau_E$ ), is crucial in the quest of reaching a burning fusion plasma [1] and accordingly the triple product is one of the central figures of merit across fusion reactor concepts [2]. The quasi-isodynamic stellarator Wendelstein 7-X (W7-X) [3] [4] [5] has been successfully optimized to reduce neoclassical heat and particle losses [6] [7], with turbulence now dominating the loss channels. Ion temperature gradient (ITG) mode driven turbulent heat transport limits the core ion temperature to 1.6 keV in most electron-cyclotron-resonance heated (ECRH) plasmas, which is known as the ion temperature clamping limit [8] and can also be present in e.g. ASDEX-Upgrade L-mode plasmas [9]. It was found that the injection of hydrogen pellets, and thereby the creation of core density gradients by core fueling in ECRH plasmas breaks the clamping limit and significantly improves the plasma performance [10] [11]. The improvement is ascribed to the stabilisation of ITG modes by the density gradient [10] [12], while trapped electron mode (TEM) type turbulence, which might otherwise be driven by such strong density gradients are stabilized by the beneficial magnetic field geometry of W7-X [13] [14] [15]. Consistent with this picture are density fluctuation measurements as a proxy of the presence of turbulence from Doppler reflectometry [16] and phase contrast imaging [17]. Another approach to create core density gradients is to make use of the core

fueling characteristic of the neutral beam injection (NBI) heating (and fueling) system [18] [19] [20] [21]. The density peaking dynamics are not trivially determined by the particle sources alone, but also by a transition to an anomalous transport regime with increased peaking rate [22], without which the desired density gradients can not be reached. In the scenario developed here [23], this transition is achieved by switching to only NBI heating in relatively high density plasmas. A simultaneous transition to a strongly suppressed anomalous transport is also seen in the impurity channel [24] [25]. The peaked electron density profiles reduce the heat diffusivity by a factor of 4 [23] but the achieved core temperatures are limited by the moderate power of the NBI system for the very high core density, which continues to rise. Reintroducing ECRH into NBI heated plasmas after reaching a certain core density gradient can raise the ion temperature above the clamping limit due to the improved core energy confinement and the strong coupling of electrons and ions [23]. The ECRH induces a core density 'pump-out' effect, slowing the development of the core density gradient, or even reducing it. When the gradient is reduced too far, a back-transition to the regime of higher particle and heat transport is observed. The pump-out effect of the ECRH is magnetic configuration dependent and not well understood for Stellarators even though it has been investigated in detail for many Tokamaks, finding a strong dependence on the collisionality and turbulence drive [26][27][28][29][30].

The stability of the density gradient is determined not only by the interplay of the 'pump-out' and the NBI particle fueling but also the recycling particle fueling and the turbulent and neoclassical particle transport, all of which are configuration dependent. The ECRH power was fine-tuned relative to the NBI power in each of the main W7-X magnetic configurations, resulting in a given maximum stable performance and the best of these delivered the record Stellarator plasma performance in terms of the the triple product.

# 2 Results

The achieved maximum triple product and  $\tau_{\rm E}$  values and also these averaged over the 1.9s long high performance (HP) phase are given in table 1. As a reference the expected energy confinement from the ISS04 stellarator scaling [31] is given and  $f_{\rm ren}$  was simply computed as  $\tau_{\rm E}/\tau_{\rm E,\,ISS04}$ . To compute the central ion density from the measured electron density, carbon was assumed to be the dominant impurity species and  $Z_{\rm eff}$ =1.3 was determined from core carbon density measurements [32] and Bremsstrahlung [33].

Table 1: Energy confinement time and triple product in high performance phase of discharge #20241204.072 in FMM\* configuration.

Parameter	Value	Error	Unit	$f_{ m ren}$
$\overline{ au_{ m E}}$	260	$\pm 15$	ms	1.14
$ au_{ m E}^{ m max}$	286	$\pm 19$	ms	1.25
$ au_{ m E,ISS04}$	227	$\pm 12$	ms	1.0
$\overline{n_{i,0}T_{i,0} au_{ m E}}$	1.12	$\pm 0.07$	$10^{20}\mathrm{m}^{-3}\mathrm{keVs}$	
$n_{i,0}T_{i,0} au_{\mathrm{E}} ^{\mathrm{max}}$	1.21	$\pm 0.12$	$10^{20}\mathrm{m}^{-3}\mathrm{keVs}$	

In figure 1 a comparison of the averaged achieved triple product in the HP phase of the presented discharge (red+yellow star, exact value see table 1) to Tokamak H-mode plasmas (data from the CICLOP DB V5.6 [34]) is shown as function of the duration of the HP phase. The used Tokamak data base covers a range of different H-mode operational regimes including advanced regimes as e.g. negative central shear, non inductive scenarios or internal transport barriers (ITB). Clearly, in W7-X significant progress was made compared to earlier experimental campaigns (OP1 and OP2.1: marked as yellow stars with gray edges) and the preceding device Wendelstein 7-AS (bold cross). Comparing to Tokamak H-mode discharges which where stable for longer than  $2\tau_{\rm E}$ , it can be seen that the achieved triple product exceeds the performance of Tokamaks with less stored magnetic field energy than W7-X (color scale) as DIII-D, ASDEX-Upgrade, KSTAR or EAST. It is even on par with some discharges from JET or TFTR which significantly more stored magnetic field energy. The magnetic field energy was simply computed as  $E_B = V B_0^2/2\mu_0$  and the ratio to the W7-X value is shown with the color scale. It is justified as a comparative measure for two reasons. Firstly, it approximately reflects the minor radius and magnetic field part of the gyro-Bohm scaling of the triple product (scaling equation see supplementary 11). Secondly, the plasma volume and the magnetic field are the main factors determining the total device cost, so that the performance achieved per stored magnetic field energy unit is an important figure. Evidently, W7-X has achieved a very competitive triple product given its size and magnetic field. A clear degradation of performance with the HP duration is seen in the Tokamak data across all machines which is largely due to the almost linear scaling of confinement time with plasma current [35] which is inversely proportional to duration given a limited maximum voltage of the central

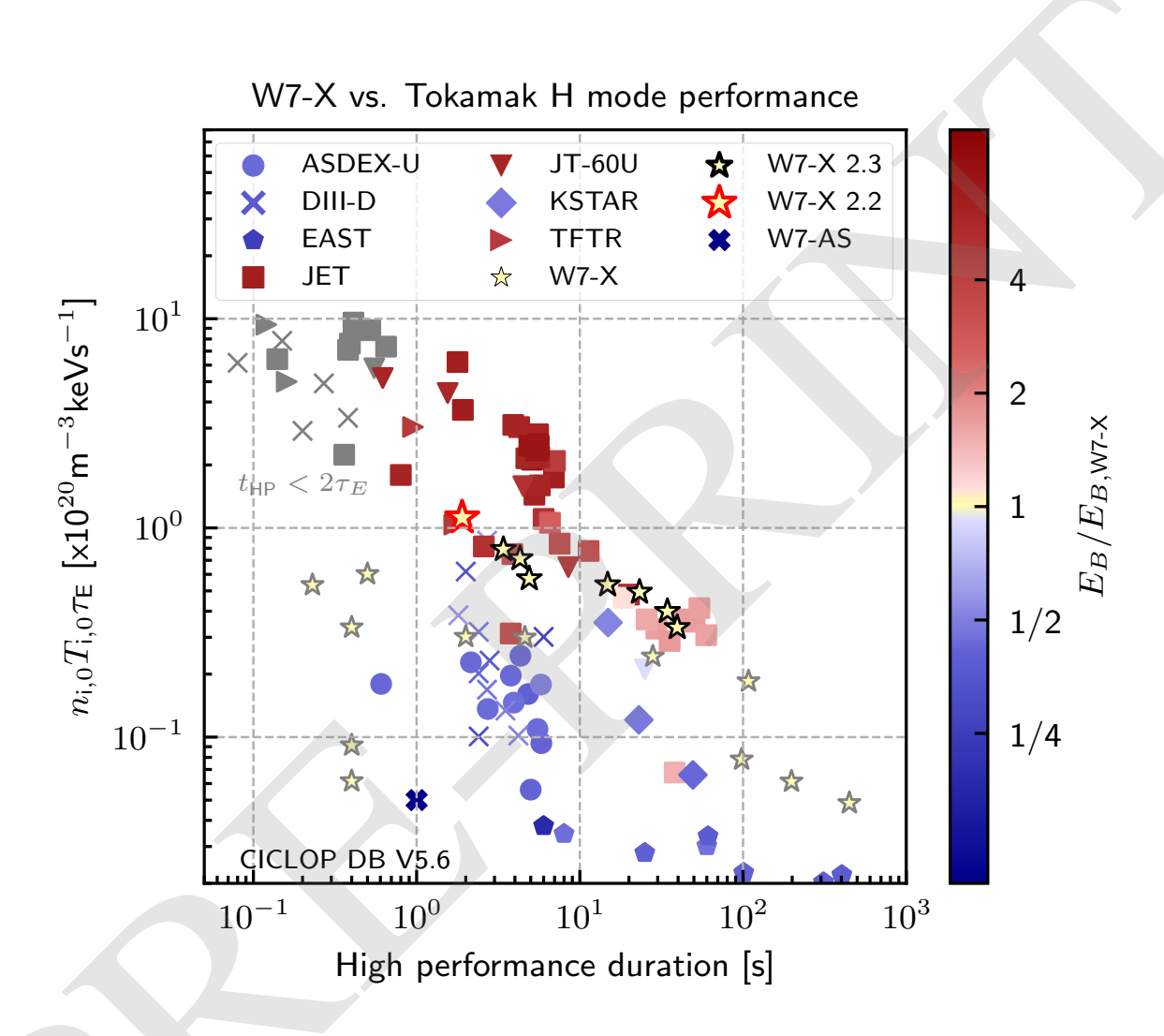


Figure 1: Triple product computed from the cental density and ion temperature plotted as function of the duration of the high performance phase. The achieved values in W7-X of the last campaigns are compared to Tokamak H mode plasmas (CICLOP DB [34]). The presented record performance achieved in OP2.2 (Discharge #20241204.072) is plotted as a red+yellow star. The color scale marks the ratio of the stored magnetic energy  $E_B = V B_0^2/2\mu_0$  in the confined region to the W7-X value.

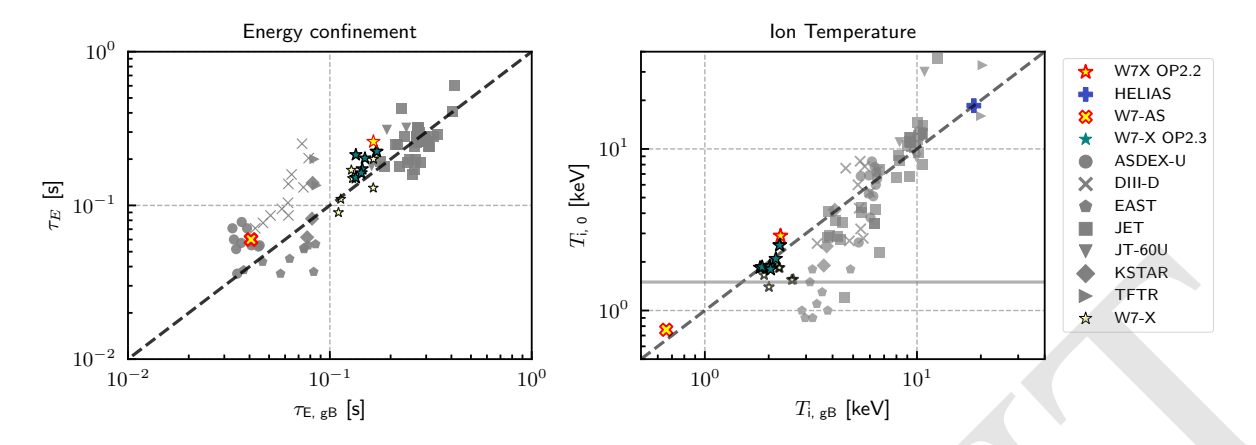


Figure 2: Left: Experimental achieved energy confinement time plotted as function of the value expected from gyro-Bohm scaling. Tokamak data points where the high performance phase was shorter than the reported energy confinement were excluded. Right: Experimental achieved core ion temperature plotted as function of the value expected from gyro-Bohm scaling. In both plots the scaling prefactor was fitted exclusively to the Tokamak data points.

solenoid. Fully or partial non-inductive current drive has been shown on several Tokamaks (e.g. AUG [36], JET [37], DIII-D[38], EAST[39]), but these typically achieve lower plasma currents and hence lower confinement. As confinement in optimised Stellarators does not depend on plasma currents, extension of the HP phase of any shown W7-X point is limited only by technical systems which are in principle steady-state capable. In the last campaign (2.3) the record shot could not be repeated or extended as it exceeded a safety limit of stored energy imposed by the configuration of the quench detection system. This has been improved for future campaigns and should allow extension of the record performance to the current limit of the W7-X NBI duration (8s). As Stellarators are less restricted to operate at high plasma densities as they are not bound by the Greenwald limit [40][41] in principle a higher triple product can be achieved by raising the density. Consequently, while the triple product is a figure of merit in its own right, additionally an analysis of the energy confinement time of the shown data points is needed for a fully informative comparison. It has been shown empirically that the Tokamak H-mode confinement and ISS04 energy confinement scale gyro-Bohm like in the normalized gyro radius  $\rho^*$  and scale only weakly with collisionality  $\nu^*$  and  $\beta$  [42] [43] [44]. Combining gyro-Bohm scaling  $\tau_{E,\mathrm{gB}} \propto (\rho^*)^{-3}$  [45] with the experimental definition  $\tau_E = \frac{W}{P_\mathrm{H}}$ , where W is the total stored plasma energy and  $P_\mathrm{H}$  is the absorbed heating power, one can readily write down the corresponding scaling of  $\tau_{E,gB}$  and  $T_{gB}$  in machine parameters (more details in supplementary or [44]):

$$T_{\rm gB} = c_1 \kappa^{-0.4} m^{-0.2} \left(\frac{P_{\rm H}}{n}\right)^{0.4} B^{0.8}$$
 (1)

$$T_{gB} = c_1 \kappa^{-0.4} m^{-0.2} \left(\frac{P_{H}}{n}\right)^{0.4} B^{0.8}$$

$$\tau_{E,gB} = c_2 a^3 \kappa^{0.6} m^{-0.2} \left(\frac{P_{H}}{n}\right)^{-0.6} B^{0.8},$$
(2)

where  $\kappa = \frac{R}{a}$  is the aspect ratio, m the isotope mass and  $c_1$  and  $c_2$  are constants which need to be determined from the data. The resulting scaling in  $\tau_{\rm E}$  is very similar to the one derived in [46] from a critical gradient Tokamak heat transport model. While this simple approach facilitates the comparison between Stellarators and Tokamaks it ignores effects of rotational transform, collisionality and  $\beta$  on confinement. Still, as can be seen in figure 2, it reproduces the general trends between machines quite well. The achieved energy confinement times (left) and central ion temperatures (right) are plotted vs the gyro-Bohm values computed using equations 1 and 2. For a consistent comparison between Tokamak and Stellarator data the minor radius a in the gyro-Bohm scaling expressions was defined via the plasma volume ( $a^2 = V/(2\pi^2 R)$ ) and accordingly the Tokamak minor radii given in the data base were adjusted as  $a=a_{\text{Tokamak}}\sqrt{\epsilon}$ , where  $\epsilon$  is the elongation factor (following [47]). The prefactors c1 and c2 have been fitted exclusively to the Tokamak data in order to show how the Stellarator results compare to a range of H-mode operational regimes. As can be seen in the left figure 2 the HP discharges of W7-X reach a similar  $\tau_E$  as e.g. JET which is due to the small heating power to density ratio in W7-X. More importantly however, comparing the best performing W7-AS discharge (red+yellow bold cross, data from [48]) to W7-X it is seen that the energy confinement follows the same scaling as in Tokamak H-mode plasmas, which is in line with the results from a more detailed comparison done in [46]. The shown W7-AS result was achieved in a so called

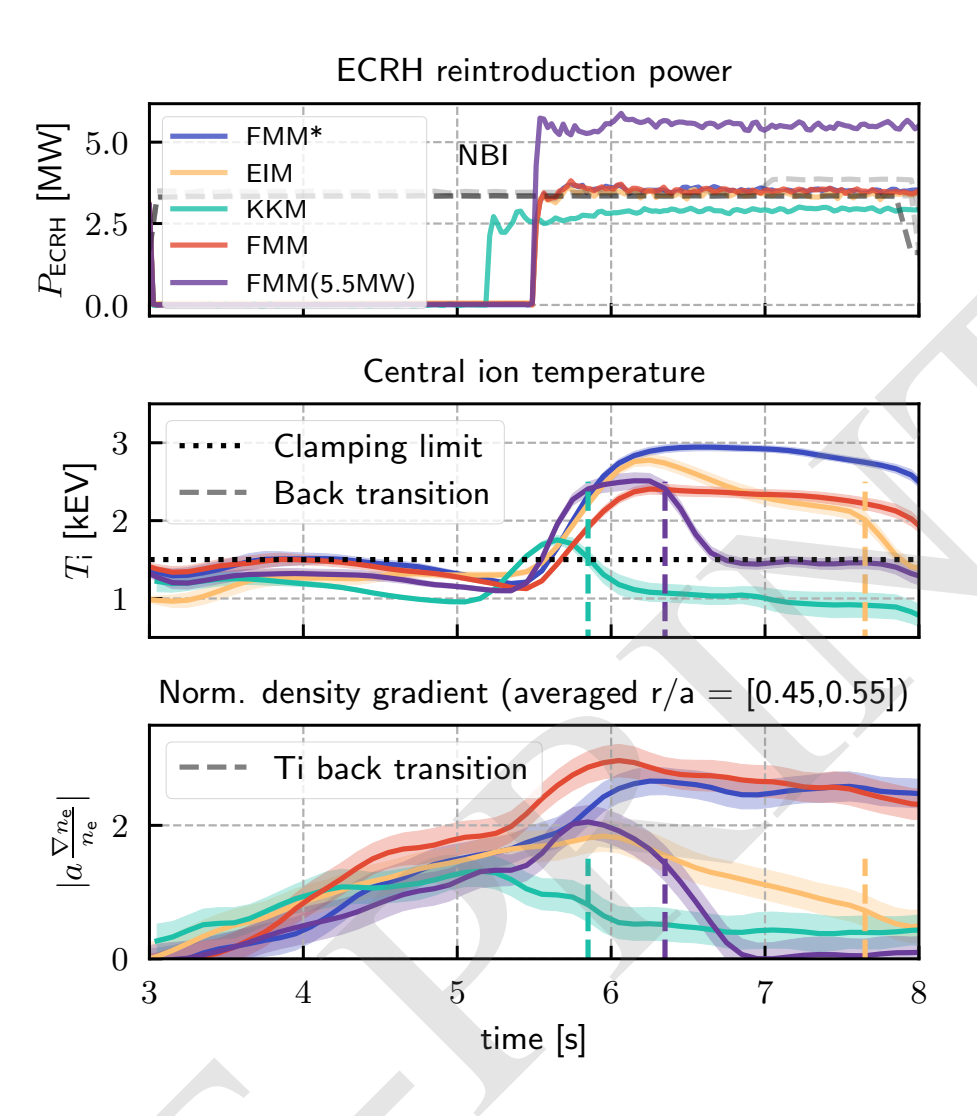


Figure 3: Top: ECRH reintroduction power of the analyzed discharges. Mid: The core ion temperature measured by the CXRS system. The dashed-dotted lines mark the back transition to a transport regime with significantly lower ion temperature. The dashed line marks the clamping temperature limit seen in ECRH discharges with flat density profiles. Bottom: Normalized density gradient scale length averaged in the radial region from r/a=0.45 to 0.55 measured with the Thomson scattering diagnostic. The dashed lines mark the time points of the transition to lower ion temperatures.

high confinement NBI discharge [49][50][51] which has strong similarities to the W7-X scenario described here. The same trend is seen in the achieved ion temperature (right figure 2), where the improvement going from W7-AS to W7-X is very well captured by the Tokamak fitted gyro-Bohm scaling. Judging from this result, it becomes apparent that the relatively low ion temperatures achieved in HP W7-X discharges are not due to bad confinement but most likely are explained by the low heating power to density ratio. Following from this, the question arises if the ratio could be easily increased. To evaluate this, it is necessary to study if the strong density gradients and resulting higher confinement of this scenario can be maintained with higher heating power. The reported record performance was achieved by adding ECRH power to a plasma with a strong core electron density gradient initially created by purely NBI heating and fueling, as described in detail in [23]. This heating scenario was developed in several magnetic configurations differing in magnetic mirror ratio and  $\iota$  profile (detailed parameters in supplementary table 2). In the top figure 3 time traces of the ECRH and NBI power over the NBI phase of the selected discharges in the investigated configurations are shown. In all cases the NBI power was ≈3.5MW while the ECRH power varied between 2.5MW to 5.5MW. The investigated configurations were the so called standard (EIM), high-mirror (KKM) and  $\iota$ -scan (FMM) configuration, which is a limiter type configuration and has islands near the edge but inside the confined region [52] [53]. Maximum performance was achieved in FMM\*, which is a FMM type configuration with additional control coil currents of  $I_C=-2.5 \mathrm{kA}$  reducing the internal island size.

In all configurations the ECRH reintroduction raised the core ion temperature, measured by the CXRS system [54], above the clamping limit (black dashed line) which is shown in figure 3 (mid). In FMM\* and standard the highest ion temperatures of  $\approx$ 2.9 keV were reached and high-mirror performed worst of all. In three of the cases (FMM with 5.5 MW ECRH (violet), EIM, KKM) a sharp and sudden fall off in the ion temperature (marked as vertical dashed lines in figure 3 mid) can be seen. As this occurred without any change in the heating it marks a transition from the low heat diffusivity seen in the high performance phase to that of a typical ECRH plasma with flat density profiles [23] [55].

During the HP phase the strongest normalized core density gradients, measured by the Thomson scattering system [56], were located between r/a=0.45 to r/a=0.55. As the exact radial location varied between configurations the average on that r/a interval is plotted in figure 3 (bottom). It can be clearly seen that the stability of the gradient depends on the added ECRH power and the magnetic configuration. At a reintroduced power of 3.5 MW the core density gradient in the FMM\* configuration (blue line) was stable while in standard (EIM, yellow line) the same power or in high-mirror (KKM, green line) even less power caused a continuous reduction of the normalized gradient until it nearly completely collapses. Generally, it was found that for each configuration the ECRH power must be fine tuned to keep the density gradient stable. Adding too much ECRH lead to a gradual reduction of the gradient until at a certain critical value it suddenly collapsed, coinciding with the transition to a higher heat diffusivity regime. Although it is globally observed that high ECRH powers eventually lead to a reduction of the core density gradients, the details of the profile evolution are more subtle. Particularly in the FMM cases, where the increased power initially lead to an increase of the gradient within the specific region shown here. A detailed investigation of the profile effects requires a radial particle transport analysis which is left for a future publication.

In figure 4 the plasma performance in terms of the experimentally measured triple product (top plot) and the energy confinement time (mid plot) are shown as time traces for FMM (red line, violet line) and FMM\* (blue). The triple product was computed from the measured, central density (Thomson scattering) and ion temperature (CXRS) values and the energy confinement time which was computed from the measured diamagnetic energy (Diamagnetic loops [57]) and heating power as  $\tau_{\rm E} = \frac{W}{P_{\rm H}-\dot{W}}$ . The triple product expected from the gyro-Bohm scaling,  $nT_{\rm gB}\tau_{\rm E,gB}$ , fitted to the already shown Tokamak H-mode data is shown as a dashed line. The increasing trend due to the rising core density during the pure NBI phase is remarkably well captured and it can be seen that, except for the constant prefactor, ISS04 and gyro-Bohm scaling show a similar time evolution for the energy confinement time. From the gyro-Bohm scaling a slight degradation of the triple product  $(\propto P_{\rm H}^{-0.2})$  and a strong degradation of the energy confinement  $(\propto P_{\rm H}^{-0.6})$  would be expected when increasing the heating power with ECRH reintroduction (at 5.5 s). However, in the FMM\* configuration (blue line) the energy confinement only decreased very shortly and then rose to its value from before over a time window of  $\approx 300$  ms, which together with the ion temperature increase yielded the significantly increased triple product. This means that either the reintroduction of ECRH improved the energy confinement regime or the plasma is in a transport regime for which no power degradation is seen. Clearly, increasing the ECRH power in FMM from 3.5 MW (red) to 5.5 M (violet) did not lead to a better performance or even higher ion temperatures (see figure 3) which is due to the strong and fast reduction of the core density gradient. The overall confinement time in FMM is lower which is most likely due to a profile flattening effect in the internal island region during the HP phase and will be studied in a dedicated publication.

# 3 Conclusion

Concluding, in Wendelstein 7-X an unprecedented Stellarator plasma performance in terms of the triple product was measured. The achieved value is in line with H-mode Tokamak discharges when taking into account the differing stored magnetic energy of the devices. Comparing to a similar high confinement discharge scenario from W7-AS [51] good agreement with the reactor favorable gyro-Bohm scaling was found. The measured energy confinement time was above the ISS04 scaling for several energy confinements times. While the improved performance could be seen across several magnetic configurations, proving the robustness of the core density gradient effect on the heat transport, it was shown that the stability of the core gradient with combined NBI+ECR heating and thereby the duration of the high performance phase strongly depends on the magnetic configuration. An open issue to be addressed in the light of the reactor relevance of the presented scenario is the strong impurity accumulation in these turbulence reduced ion root plasma regimes [24][25].

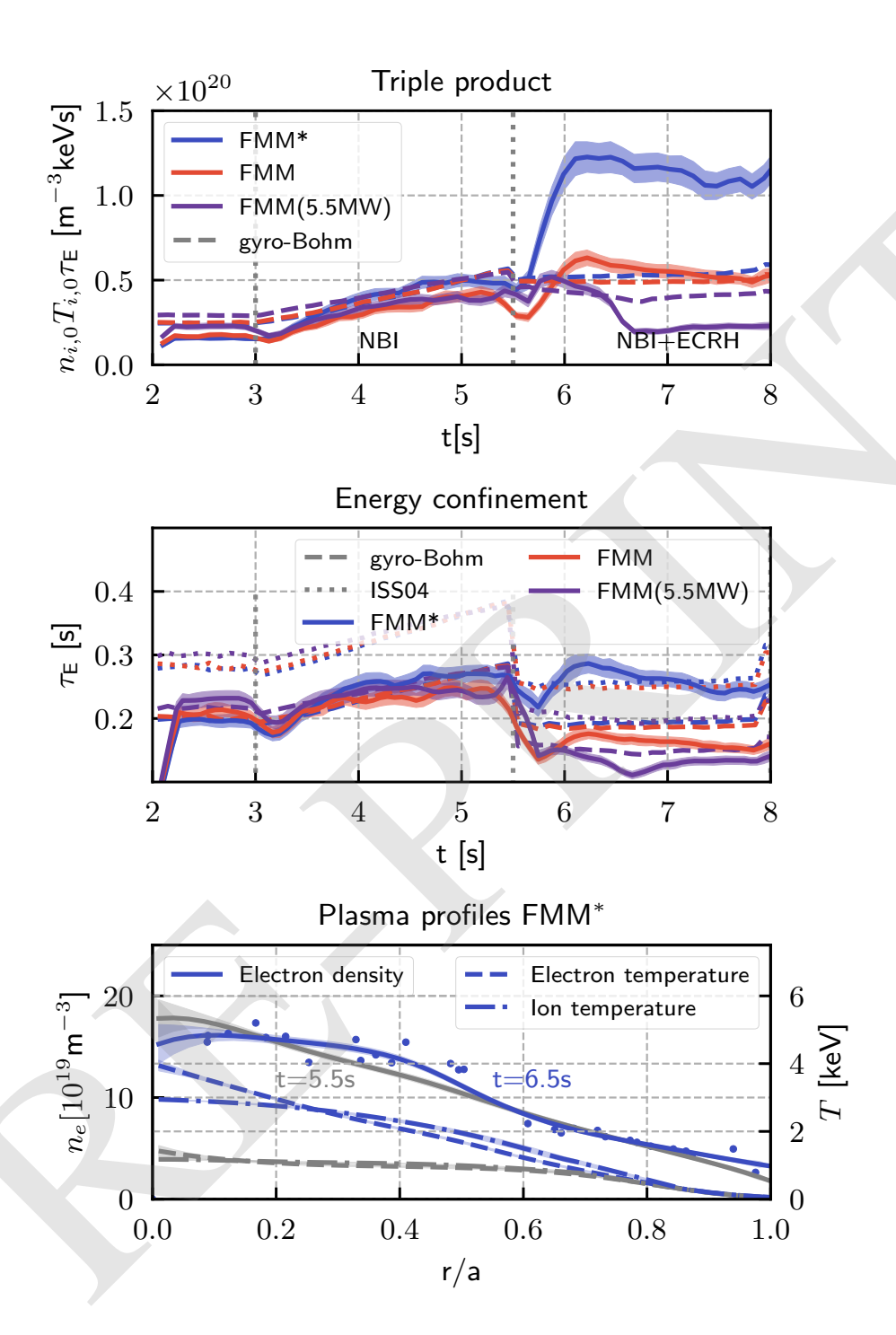


Figure 4: Plasma performance time trace over the NBI phase of #20241204.072 in the FMM\* magnetic configuration and #20241204.063 (red) and #20241126.073 (violet) in the FMM configuration. From 5.5s to 8s the plasma is heated by combined 3.4 MW NBI and 3.5 MW (blue, red) or 5.5 MW (violet) ECRH. Top: Triple product over time computed from the central electron density and ion temperature. Mid: The experimental energy confinement time (blue line) compared to the ISS04 scaling (dotted line) [31] and gyro-Bohm scaling fitted to Tokamak H-mode data (dashed line). Bottom: Plasma profiles in FMM\* configuration (#20241204.072) in HP phase at 6.5 s (blue) and right before ECRH reintroduction at 5.5 s (gray). For the electron density (solid line) the Thomson scattering data points as measured are shown as a reference (blue dots)

# **Supplementary**

# **Magnetic configurations**

Table 2: Magnetic configuration parameters

Mag. conf.	$\iota_{2/3}$	$\epsilon_{ m eff,1/2}$	a [m]	ID
FMM	0.952	0.0075	0.55	20241126.073
				20241204.063
FMM*	0.942	0.0069	0.55	20241204.072
EIM ('standard')	0.881	0.0061	0.52	20241205.066
KKM ('high-mirror')	0.899	0.0216	0.51	20230323.038

#### 4.2 Plasma profiles

The electron density and temperature profiles were obtained using the Thomson scattering diagnostic [56]. The electron density profile was renormalized using the line integrated density provided by the interferometer system [58]. Ion temperature profiles were obtained using the charge-exchange recombination spectroscopy system (CXRS) [54]. The profile mapping was done using VMEC [59][60] runs with consistent pressure profiles, thereby including  $\beta$  effects on the equilibrium.

### **Gyro-Bohm scaling**

Assuming dominant heat transport gyro-Bohm scaling in  $\rho^*$  (ITG) and weak dependence on  $\beta$  and  $\nu^*$  as in Tokamak H mode [42]:

$$\omega \tau_{E,gb} \propto (\rho^*)^{-3} \tag{3}$$

$$\omega = \frac{qB}{2\pi m} \tag{4}$$

$$\omega \tau_{E,gb} \propto (\rho^*)^{-3}$$

$$\omega = \frac{qB}{2\pi m}$$

$$\rho^* = \frac{\rho_L}{a} = \frac{mv_\perp}{a \cdot qB} = \frac{(2kTm)^{\frac{1}{2}}}{a \cdot qB}$$

$$v_\perp = \frac{2}{3}v_{th}$$

$$(3)$$

$$(4)$$

$$(5)$$

$$v_{\perp} = \frac{2}{3}v_{\rm th} \tag{6}$$

$$\tau_{E,gb} \propto \frac{1}{\omega} \left( \frac{(2kTm)^{\frac{1}{2}}}{a \cdot qB} \right)^{-3} \propto m^{-\frac{1}{2}} T^{-\frac{3}{2}} a^3 q^2 B^2$$
(7)

Combining with the definition of  $\tau_{\rm E}$  via the kinetic profiles and heating power

$$\tau_{\rm E} = \frac{W}{P_{\rm H}} = \frac{3nkT}{P_{\rm H}} \tag{8}$$

gyro-Bohm scalings for T and  $\tau_E$  can be written in terms of geometric quantities, density n and heating power  $P_H$ :

$$T_{\rm gB} = c_1 \kappa^{-0.4} m^{-0.2} \left(\frac{P_{\rm H}}{n}\right)^{0.4} B^{0.8}$$
 (9)

$$\tau_{E,gB} = c_2 a^3 \kappa^{0.6} m^{-0.2} \left(\frac{P_{\rm H}}{n}\right)^{-0.6} B^{0.8} \tag{10}$$

Consequently, if gyro-Bohm scaling holds the triple product F scales as:

$$F \propto a^3 \kappa^{0.2} m^{-0.4} n^{1.2} P_{\rm H}^{-0.2} B^{1.6} \tag{11}$$

# References

[1] J D Lawson. "Some Criteria for a Power Producing Thermonuclear Reactor". In: Proceedings of the Physical Society. Section B 70.1 (Jan. 1957), p. 6. DOI: 10.1088/0370-1301/70/1/303. URL: https: //dx.doi.org/10.1088/0370-1301/70/1/303.

- [2] Samuel E. Wurzel and Scott C. Hsu. "Progress toward fusion energy breakeven and gain as measured against the Lawson criterion". In: *Physics of Plasmas* 29.6 (June 2022), p. 062103. ISSN: 1070-664X. DOI: 10.1063/5.0083990. URL: https://doi.org/10.1063/5.0083990.
- [3] G. Grieger and I. Milch. "Das Fusionsexperiment WENDELSTEIN 7-X". In: *Physikalische Blätter* 49.11 (1993), pp. 1001–1005. DOI: https://doi.org/10.1002/phbl.19930491106. URL: https://onlinelibrary.wiley.com/doi/abs/10.1002/phbl.19930491106.
- [4] R.C. Wolf et al. "Major results from the first plasma campaign of the Wendelstein 7-X stellarator". In: Nuclear Fusion 57.10 (July 2017), p. 102020. DOI: 10.1088/1741-4326/aa770d. URL: https://dx.doi.org/10.1088/1741-4326/aa770d.
- [5] T Klinger et al. "Performance and properties of the first plasmas of Wendelstein 7-X". In: *Plasma Physics and Controlled Fusion* 59.1 (Oct. 2016), p. 014018. DOI: 10.1088/0741-3335/59/1/014018. URL: https://doi.org/10.1088%2F0741-3335%2F59%2F1%2F014018.
- [6] C. Beidler et al. "PHYSICS AND ENGINEERING DESIGN FOR WENDELSTEIN VII-X". In: Fusion Technology. Stellarator systems 17 (1989).
- [7] C. D. Beidler et al. "Demonstration of reduced neoclassical energy transport in Wendelstein 7-X". In: *Nature* 596.7871 (Aug. 2021), pp. 221–226. ISSN: 1476-4687. URL: https://doi.org/10.1038/s41586-021-03687-w.
- [8] M.N.A. Beurskens et al. "Ion temperature clamping in Wendelstein 7-X electron cyclotron heated plasmas". In: *Nuclear Fusion* 61.11 (Oct. 2021), p. 116072. DOI: 10.1088/1741-4326/ac1653. URL: https://dx.doi.org/10.1088/1741-4326/ac1653.
- [9] M.N.A. Beurskens et al. "Confinement in electron heated plasmas in Wendelstein 7-X and ASDEX Upgrade; the necessity to control turbulent transport". In: *Nuclear Fusion* 62.1 (Dec. 2021), p. 016015. DOI: 10.1088/1741-4326/ac36f1. URL: https://dx.doi.org/10.1088/1741-4326/ac36f1.
- [10] S.A. Bozhenkov et al. "High-performance plasmas after pellet injections in Wendelstein 7-X". In: *Nuclear Fusion* 60.6 (Apr. 2020), p. 066011. DOI: 10.1088/1741-4326/ab7867. URL: https://dx.doi.org/10.1088/1741-4326/ab7867.
- [11] T. Klinger et al. "Overview of first Wendelstein 7-X high-performance operation". In: *Nuclear Fusion* 59.11 (June 2019), p. 112004. DOI: 10.1088/1741-4326/ab03a7. URL: https://dx.doi.org/10.1088/1741-4326/ab03a7.
- [12] Wendell Horton. Turbulent transport in magnetized plasmas. World Scientific, 2012.
- [13] J. H. E. Proll et al. "Resilience of Quasi-Isodynamic Stellarators against Trapped-Particle Instabilities". In: *Phys. Rev. Lett.* 108 (24 June 2012), p. 245002. DOI: 10.1103/PhysRevLett.108.245002. URL: https://link.aps.org/doi/10.1103/PhysRevLett.108.245002.
- [14] G. G. Plunk et al. "Stellarators Resist Turbulent Transport on the Electron Larmor Scale". In: *Phys. Rev. Lett.* 122 (3 Jan. 2019), p. 035002. DOI: 10.1103/PhysRevLett.122.035002. URL: https://link.aps.org/doi/10.1103/PhysRevLett.122.035002.
- [15] J A Alcusón et al. "Suppression of electrostatic micro-instabilities in maximum-J stellarators". In: *Plasma Physics and Controlled Fusion* 62.3 (Jan. 2020), p. 035005. DOI: 10.1088/1361-6587/ab630e. URL: https://dx.doi.org/10.1088/1361-6587/ab630e.
- [16] D. Carralero et al. "An experimental characterization of core turbulence regimes in Wendelstein 7-X". In: *Nuclear Fusion* 61.9 (Aug. 2021), p. 096015. DOI: 10.1088/1741-4326/ac112f. URL: https://dx.doi.org/10.1088/1741-4326/ac112f.
- [17] A. v. Stechow et al. "Suppression of core turbulence by profile shaping in Wendelstein 7-X". In: (2020). arXiv: 2010.02160 [physics.plasm-ph]. URL: https://arxiv.org/abs/2010.02160.
- [18] P. McNeely et al. "Current status of the neutral beam heating system of W7-X". In: Fusion Engineering and Design 88.6 (2013). Proceedings of the 27th Symposium On Fusion Technology (SOFT-27); Liège, Belgium, September 24-28, 2012, pp. 1034–1037. ISSN: 0920-3796. DOI: https://doi.org/10.1016/j.fusengdes.2013.03.006. URL: http://www.sciencedirect.com/science/article/pii/S0920379613003001.
- [19] Samuel A. Lazerson et al. "First neutral beam experiments on Wendelstein 7-X". In: *Nuclear Fusion* 61.9 (July 2021), p. 096008. DOI: 10.1088/1741-4326/ac121c. URL: https://dx.doi.org/10.1088/1741-4326/ac121c.

- [20] Samuel A. Lazerson et al. "Validation of the BEAMS3D neutral beam deposition model on Wendelstein 7-X". In: *Nuclear Fusion* 60.7 (June 2020), p. 076020. DOI: 10.1088/1741-4326/ab8e61. URL: https://doi.org/10.1088%2F1741-4326%2Fab8e61.
- [21] S. Bannmann et al. "Fast forward modeling of neutral beam injection and halo formation including full Balmer- $\alpha$  emission prediction at W7-X". In: *Journal of Instrumentation* 18.10 (Oct. 2023), P10029. DOI: 10.1088/1748-0221/18/10/P10029. URL: https://dx.doi.org/10.1088/1748-0221/18/10/P10029.
- [22] S. Bannmann et al. "Particle transport in reduced turbulence neutral beam heated discharges at Wendelstein 7-X". In: *Nuclear Fusion* 64.10 (Aug. 2024), p. 106015. DOI: 10.1088/1741-4326/ad6b37. URL: https://dx.doi.org/10.1088/1741-4326/ad6b37.
- [23] O.P. Ford et al. "Turbulence-reduced high-performance scenarios in Wendelstein 7-X". In: *Nuclear Fusion* 64.8 (July 2024), p. 086067. DOI: 10.1088/1741-4326/ad5e99. URL: https://dx.doi.org/10.1088/1741-4326/ad5e99.
- [24] T. Romba et al. "Suppression of anomalous impurity transport in NBI-heated W7-X plasmas". In: *Nuclear Fusion* 63.7 (June 2023), p. 076023. DOI: 10.1088/1741-4326/acd5e1. URL: https://dx.doi.org/10.1088/1741-4326/acd5e1.
- [25] Thilo Romba et al. "The suppression of anomalous impurity transport above a critical normalized density gradient scale length in Wendelstein 7-X". In: *Plasma Physics and Controlled Fusion* (2025). URL: http://iopscience.iop.org/article/10.1088/1361-6587/add597.
- [26] C. Angioni et al. "Density Peaking, Anomalous Pinch, and Collisionality in Tokamak Plasmas". In: *Phys. Rev. Lett.* 90 (20 May 2003), p. 205003. DOI: 10.1103/PhysRevLett.90.205003. URL: https://link.aps.org/doi/10.1103/PhysRevLett.90.205003.
- [27] C. Angioni et al. "Density response to central electron heating: theoretical investigations and experimental observations in ASDEX Upgrade". In: *Nuclear Fusion* 44.8 (June 2004), p. 827. DOI: 10.1088/0029-5515/44/8/003. URL: https://dx.doi.org/10.1088/0029-5515/44/8/003.
- [28] C Angioni et al. "Particle transport in tokamak plasmas, theory and experiment". In: *Plasma Physics and Controlled Fusion* 51.12 (Nov. 2009), p. 124017. DOI: 10.1088/0741-3335/51/12/124017. URL: https://dx.doi.org/10.1088/0741-3335/51/12/124017.
- [29] X. Wang et al. "Understanding ECH density pump-out in DIII-D H-mode plasmas". In: *Nuclear Fusion* 57.11 (Aug. 2017), p. 116046. DOI: 10.1088/1741-4326/aa7f99. URL: https://dx.doi.org/10.1088/1741-4326/aa7f99.
- [30] A Zabolotsky, H Weisen, and TCV Team. "Density profile peaking in the presence of ECRH heating in TCV". In: *Plasma Physics and Controlled Fusion* 48.3 (Jan. 2006), p. 369. DOI: 10.1088/0741-3335/48/3/003. URL: https://dx.doi.org/10.1088/0741-3335/48/3/003.
- [31] H. Yamada et al. "Characterization of energy confinement in net-current free plasmas using the extended International Stellarator Database". In: *Nuclear Fusion* 45.12 (Nov. 2005), p. 1684. DOI: 10.1088/0029-5515/45/12/024. URL: https://dx.doi.org/10.1088/0029-5515/45/12/024.
- [32] Thilo Romba. "Validation of the W7-X CXRS for impurity density profiles". MA thesis. TU Eindhoven, 2021. URL: https://pure.tue.nl/ws/portalfiles/portal/194477468/1410342\_Romba\_T.\_MSc\_thesis\_Thesis\_MAP\_MNF.pdf.
- [33] A. Pavone et al. "Measurements of visible bremsstrahlung and automatic Bayesian inference of the effective plasma charge Zeff at W7-X". In: *Journal of Instrumentation* 14.10 (Oct. 2019), p. C10003. DOI: 10. 1088 / 1748 0221 / 14 / 10 / C10003. URL: https://dx.doi.org/10.1088 / 1748 0221/14/10/C10003.
- [34] X. Litaudon et al. "Long plasma duration operation analyses with an international multi-machine (tokamaks and stellarators) database". In: *Nuclear Fusion* 64.1 (Nov. 2023), p. 015001. DOI: 10.1088/1741-4326/ad0606. URL: https://dx.doi.org/10.1088/1741-4326/ad0606.
- [35] ITER Physics Expert Group on Confinement et al. "Chapter 2: Plasma confinement and transport". In: *Nuclear Fusion* 39.12 (Dec. 1999), p. 2175. DOI: 10.1088/0029-5515/39/12/302. URL: https://dx.doi.org/10.1088/0029-5515/39/12/302.
- [36] A. Bock et al. "Non-inductive improved H-mode operation at ASDEX Upgrade". In: *Nuclear Fusion* 57.12 (Oct. 2017), p. 126041. DOI: 10.1088/1741-4326/aa8967. URL: https://dx.doi.org/10.1088/1741-4326/aa8967.

- [37] X. Litaudon et al. "Progress towards steady-state operation and real-time control of internal transport barriers in JET". In: *Nuclear Fusion* 43.7 (June 2003), p. 565. DOI: 10.1088/0029-5515/43/7/309. URL: https://dx.doi.org/10.1088/0029-5515/43/7/309.
- [38] A. M. Garofalo et al. "Access to sustained high-beta with internal transport barrier and negative central magnetic shear in DIII-Da)". In: *Physics of Plasmas* 13.5 (May 2006), p. 056110. ISSN: 1070-664X. DOI: 10.1063/1.2185010.eprint: https://pubs.aip.org/aip/pop/article-pdf/doi/10. 1063/1.2185010/15805073/056110\\_1\\_online.pdf. URL: https://doi.org/10.1063/1.2185010.
- [39] B.N. Wan et al. "Recent advances in EAST physics experiments in support of steady-state operation for ITER and CFETR". In: *Nuclear Fusion* 59.11 (June 2019), p. 112003. DOI: 10.1088/1741-4326/ab0396. URL: https://dx.doi.org/10.1088/1741-4326/ab0396.
- [40] Martin Greenwald. "Density limits in toroidal plasmas". In: *Plasma Physics and Controlled Fusion* 44.8 (July 2002), R27. DOI: 10.1088/0741-3335/44/8/201. URL: https://dx.doi.org/10.1088/0741-3335/44/8/201.
- [41] P Helander et al. "Stellarator and tokamak plasmas: a comparison". In: *Plasma Physics and Controlled Fusion* 54.12 (Nov. 2012), p. 124009. DOI: 10.1088/0741-3335/54/12/124009. URL: https://doi.org/10.1088%2F0741-3335%2F54%2F12%2F124009.
- [42] J.G. Cordey et al. "Scaling of the energy confinement time with  $\beta$  and collisionality approaching ITER conditions". In: *Nuclear Fusion* 45.9 (Aug. 2005), p. 1078. DOI: 10.1088/0029-5515/45/9/007. URL: https://dx.doi.org/10.1088/0029-5515/45/9/007.
- [43] A. Dinklage et al. "Assessment of Global Stellarator Confinement: Status of the International Stellarator Confinement Database". In: Fusion Science and Technology 51.1 (2007), pp. 1–7. DOI: 10.13182/FST07-A1281. URL: https://doi.org/10.13182/FST07-A1281.
- [44] J. Miyazawa et al. "Characteristics of the Global Energy Confinement and Central Pressure in LHD". In: *Fusion Science and Technology* **58.1** (2010), pp. 29–37. DOI: 10.13182/FST10-A10790. URL: https://doi.org/10.13182/FST10-A10790.
- [45] G. Manfredi and M. Ottaviani. "Gyro-Bohm Scaling of Ion Thermal Transport from Global Numerical Simulations of Ion-Temperature-Gradient-Driven Turbulence". In: *Phys. Rev. Lett.* 79 (21 Nov. 1997), pp. 4190–4193. DOI: 10.1103/PhysRevLett.79.4190. URL: https://link.aps.org/doi/10.1103/PhysRevLett.79.4190.
- [46] U. Stroth et al. "Stellarator-tokamak energy confinement comparison based on ASDEX Upgrade and Wendelstein 7-X hydrogen plasmas". In: *Nuclear Fusion* 61.1 (Nov. 2020), p. 016003. DOI: 10.1088/1741-4326/abbc4a. URL: https://dx.doi.org/10.1088/1741-4326/abbc4a.
- [47] U. Stroth et al. "Energy confinement scaling from the international stellarator database". In: *Nuclear Fusion* 36.8 (Aug. 1996), p. 1063. DOI: 10.1088/0029-5515/36/8/II1. URL: https://dx.doi.org/10.1088/0029-5515/36/8/II1.
- [48] F. Wagner et al. "W7-AS: One step of the Wendelstein stellarator linea)". In: *Physics of Plasmas* 12.7 (June 2005), p. 072509. ISSN: 1070-664X. DOI: 10.1063/1.1927100. URL: https://doi.org/10.1063/1.1927100.
- [49] U Stroth et al. "High-confinement NBI discharges in the W7-AS stellarator". In: *Plasma Physics and Controlled Fusion* 40.8 (Aug. 1998), p. 1551. DOI: 10.1088/0741-3335/40/8/008. URL: https://dx.doi.org/10.1088/0741-3335/40/8/008.
- [50] M Kick et al. "Electric field and transport in W7-AS". In: *Plasma Physics and Controlled Fusion* 41.3A (Mar. 1999), A549. DOI: 10.1088/0741-3335/41/3A/048. URL: https://dx.doi.org/10.1088/0741-3335/41/3A/048.
- [51] M Hirsch et al. "Major results from the stellarator Wendelstein 7-AS". In: *Plasma Physics and Controlled Fusion* 50.5 (Mar. 2008), p. 053001. DOI: 10.1088/0741-3335/50/5/053001. URL: https://dx.doi.org/10.1088/0741-3335/50/5/053001.
- [52] T. Andreeva et al. "Magnetic configuration scans during divertor operation of Wendelstein 7-X". In: *Nuclear Fusion* 62.2 (Jan. 2022), p. 026032. DOI: 10.1088/1741-4326/ac3f1b. URL: https://dx.doi.org/10.1088/1741-4326/ac3f1b.
- [53] N. Chaudhary et al. "Electron transport barrier and high confinement in configurations with internal islands close to the plasma edge of W7-X". In: *Nuclear Fusion* 64.10 (Sept. 2024), p. 106038. DOI: 10.1088/1741-4326/ad703e. URL: https://dx.doi.org/10.1088/1741-4326/ad703e.

- [54] O. P. Ford et al. "Charge exchange recombination spectroscopy at Wendelstein 7-X". In: *Review of Scientific Instruments* 91.2 (2020), p. 023507. DOI: 10.1063/1.5132936.
- [55] M Wappl et al. "Experimental power balance study on turbulent heat transport at Wendelstein 7-X". In: *Plasma Physics and Controlled Fusion* 67.7 (July 2025), p. 075025. DOI: 10.1088/1361-6587/ade824. URL: https://dx.doi.org/10.1088/1361-6587/ade824.
- [56] S.A. Bozhenkov et al. "The Thomson scattering diagnostic at Wendelstein 7-X and its performance in the first operation phase". In: *Journal of Instrumentation* 12.10 (Oct. 2017), P10004. DOI: 10.1088/1748-0221/12/10/P10004. URL: https://dx.doi.org/10.1088/1748-0221/12/10/P10004.
- [57] K. Rahbarnia et al. "Diamagnetic energy measurement during the first operational phase at the Wendelstein 7-X stellarator". In: *Nuclear Fusion* 58.9 (July 2018), p. 096010. DOI: 10.1088/1741-4326/aacab0. URL: https://dx.doi.org/10.1088/1741-4326/aacab0.
- [58] K.J. Brunner et al. "Real-time dispersion interferometry for density feedback in fusion devices". In: *Journal of Instrumentation* 13.09 (Sept. 2018), P09002. DOI: 10.1088/1748-0221/13/09/P09002. URL: https://dx.doi.org/10.1088/1748-0221/13/09/P09002.
- [59] M. Grahl et al. "Web Services for 3D MHD Equilibrium Data at Wendelstein 7-X". In: *IEEE Transactions on Plasma Science* 46.5 (2018), pp. 1114–1119. DOI: 10.1109/TPS.2017.2784903.
- [60] S.P. Hirshman, W.I. van RIJ, and P. Merkel. "Three-dimensional free boundary calculations using a spectral Green's function method". In: *Computer Physics Communications* 43.1 (1986), pp. 143–155. ISSN: 0010-4655. DOI: https://doi.org/10.1016/0010-4655 (86) 90058-5. URL: http://www.sciencedirect.com/science/article/pii/0010465586900585.